Biofunctionalized Titanium Dioxide Nanoparticles with Bovine Serum Albumin for Targeted Cytotoxicity in MCF-7 Breast Cancer Cells

Sanam Rahujo[1*], Farah Naz Talpur[1], Abdul Qadeer Laghari[2], Olcay Mert[3], Hassan Imran Afridi[1], Zafar Ali[4], Noshad Razzaque[1], Imamdin Chandio[5], Noor Zaman[1], and Masroor Abro[2]**

[1]*National Center of Excellence in Analytical Chemistry, University of Sindh, Jamshoro 76080, Pakistan*

[2]*Department of Chemical Engineering, Mehran University of Engineering and Technology, Jamshoro 76062, Pakistan*

[3]*Department of Chemistry, Faculty of Arts and Science, Kocaeli University, Kocaeli 413805, Turkey*

[4]*Department of Chemistry, Faculty of Science, Engineering and IT, University of Turbat, Balochistan 75700, Pakistan*

[5]*MOE Key Laboratory of Bioorganic Phosphorus Chemistry and Chemical Biology, Department of Chemistry, Tsinghua University, Beijing 100084, China*

*** Corresponding author:**

tel: +92-3113586849
email: sanamrahujo@yahoo.com; abdul.qadeer@admin.muet.edu.pk***

Received: July 25, 2025
Accepted: November 17, 2025

DOI: 10.22146/ijc.109676

Abstract: *The titanium dioxide nanoparticles (TiO_2NPs) were synthesized and functionalized with bovine serum albumin (BSA) to yield TiO_2@BSA nanocomposites for targeted drug delivery. The chemotherapeutic drug vinorelbine (VRL), used for non-small cell lung and breast cancer, was loaded into the nanocomposites by a cost-efficient sol-gel method. The UV-vis spectrum exhibited an absorption peak at 361 nm, confirming the formation of TiO_2 NPs. In the FTIR spectrum, the grafting of BSA was indicated by specific band shifts. XRD and FESEM revealed well-dispersed spherical particles with an average crystallite size of ~20 nm, and EDX confirmed elemental composition. The zeta potential of −29 mV indicated colloidal stability with a drug loading efficiency of 62%.* In vitro *release studies demonstrated pH-responsive behavior, with 98% cumulative release at an acidic pH (5.5) compared to 20% at physiological pH (7.4), indicating the suitability of this formulation for tumor-targeted delivery. Higuchi and Korsmeyer-Peppas models were used for the kinetics study, indicating that the mechanism was controlled by diffusion and swelling. Cytotoxicity evaluation via MTT assay showed enhanced uptake and anticancer activity of VRL-loaded TiO_2@BSANPs against MCF-7 cells compared with free VRL. These results suggest TiO_2@BSA nanocarriers as efficient, stable, and selective platforms for cancer therapy.*

Keywords: *bovine serum albumin; titanium dioxide nanoparticles; targeted drug delivery; breast cancer; vinorelbine drug*

■ INTRODUCTION

Cancer, characterized by uncontrolled cell proliferation, remains a leading cause of mortality worldwide. Among women, breast cancer (BC) is the most commonly diagnosed malignancy, with over a million new cases reported annually [1]. Advanced and metastatic BC forms present significant treatment challenges [2]. Conventional treatments such as surgery, radiotherapy, and chemotherapy are often limited by non-specific drug distribution, which results in systemic toxicity and reduced efficacy [3]. To overcome these limitations, targeted drug delivery systems have been developed to enhance drug accumulation at tumor sites and reduce off-target effects. Nanocarriers, such as liposomes, dendrimers, and polymeric nanoparticles, have shown promise; however, challenges related to cost, complexity, and scalability hinder their clinical application. In contrast, inorganic nanoparticles, such as titanium dioxide nanoparticles (TiO_2NPs), offer advantages including ease of synthesis, biocompatibility,

chemical stability, and cost-effectiveness [4]. Selection of suitable coating materials is essential for ensuring nanoparticle stability, as stabilizing agents generate repulsive interactions between particles and prevent aggregation [5]. Bovine serum albumin (BSA) coating improves nanoparticle dispersion in aqueous environments, enhances functionality, and increases the efficiency of vinorelbine (VRL) delivery into tumor cells. Serum albumins, the predominant proteins in blood plasma, perform diverse physiological roles. Owing to its high structural and sequence similarity to human serum albumin, BSA is one of the most extensively studied proteins and is considered an excellent candidate for biocompatible nanoparticle coatings in biomedical applications. Maintaining the natural conformation of albumin during surface attachment enhances blood compatibility, prolongs circulation time, and minimizes nonspecific protein adsorption.

TiO_2NPs have been investigated for various therapeutic applications [6], including photodynamic and sonodynamic therapies. Among synthesis approaches, the sol–gel method is favored for producing uniform, high-purity TiO_2NPs at relatively low temperatures [7]. Surface functionalization enhances dispensability and drug-loading capacity, and proteins such as BSA are widely utilized due to their biocompatibility, which inhibits aggregation, improves drug solubility and stability, facilitates passive tumor targeting, and exhibits low immunogenicity. It is a safe and efficient carrier when coated onto metal nanoparticles for drug delivery. Improved drug loading, release, and therapeutic efficacy, particularly in cancer treatment, are facilitated by BSA's diverse ligand binding capabilities and well-understood pharmacokinetics. BSA is a globular protein of ~66.5 kDa composed of 583 amino acids and stabilized by disulfide bonds [8]. BSA carries a net charge of ~185 ions per molecule at physiological pH, conferring high solubility and a strong binding ability to drugs, lipids, and metal ions, making it widely used in biochemistry and nanomaterial research.

VRL, a semi-synthetic Vinca alkaloid, disrupts microtubule dynamics and is widely used in BC therapy [9]. However, its nonspecific delivery may induce adverse effects, such as phlebitis. Current carriers, including liposomes, often face limitations such as instability, high cost, and rapid clearance, underscoring the need for more effective systems. This study reports the synthesis of TiO_2NPs by the sol–gel method, followed by BSA surface modification to produce TiO_2@BSA nanocomposites. These nanocomposites were employed for VRL loading, pH-responsive release evaluation, and cytotoxicity testing against MCF-7 BC cells. The BSA coating enhanced biocompatibility and facilitated controlled release, thereby highlighting TiO_2@BSA as a promising platform for targeted BC therapy with reduced systemic toxicity.

■ EXPERIMENTAL SECTION

Materials

Titanium(IV) isopropoxide, BSA, phosphate buffer, glacial acetic acid, and 3-(4,5-dimethylthiazol-2-yl)-2,5-diphenyltetrazolium bromide (MTT) were procured from Sigma-Aldrich, Darmstadt, Germany. Dimethyl sulfoxide (DMSO) was purchased from Fisher Scientific (Waltham, MA, USA). The human breast cancer cell line MCF-7 was obtained from ATCC® HTB-22™ (Manassas, VA, USA). At the same time, the anticancer drug VRL was donated by the Department of Clinical Oncology, Nuclear Institute of Medicine & Radiotherapy (NIMRA), Liaquat University of Medical and Health Sciences (LUMHS), Jamshoro, Sindh, Pakistan.

Instrumentation

The absorption spectra of the TiO_2@BSANPs solution were captured using a PerkinElmer Lambda 365 Spectrophotometer for UV-vis measurements in the 200–800 nm wavelength range. TiO_2@BSANPs were analyzed using a Thermo Nicolet FTIR spectrometer (model 5700, USA) with KBr pellets. A detachable ZnSe crystal was attached to the sample chamber via an attenuated total reflectance (ATR) attachment to obtain Fourier-transform infrared (FTIR) spectrum. Bruker's XRD model D8, from Germany, was used to verify the crystalline texture and size of the synthesized particles. A JEOL field emission scanning electron microscope instrument, model 5800LV (Tokyo, Japan), was utilized

to examine the surface morphology of the particles. The size of nanoparticles in solution and their zeta potential were determined using the Zeta-Sizer model, Nano-ZS from Malvern.

Procedure

Preparation of TiO_2@BSANPs

The TiO_2@BSA nanocomposites were synthesized following the procedure reported previously [10]. Briefly, 0.5 g of titanium(IV) isopropoxide was dissolved in 100 mL of distilled water containing 5 mL of glacial acetic acid. Subsequently, a BSA solution (0.5 g of BSA in 15 mL of deionized water) was added dropwise to the precursor mixture, which was stirred continuously. The resulting solution was heated and stirred at 80 °C for 5 h. The obtained suspension was centrifuged at 8,000 rpm for 10 min, and the white precipitate was collected. It was then washed several times with deionized water (2–3 times) and once with methanol. The product was dried overnight in an oven at 80 °C, then finely ground, and subsequently calcined at 500 °C for 5 h. The overall research framework, including the synthesis of TiO_2@BSANPs, their characterization, VRL loading and release, as well as evaluation in breast cancer cell lines, is schematically presented in Fig. 1.

Drug loading

The drug loading capacity was calculated by adding 1 mL of a 100 ppm VRL solution to 2 mg of TiO_2@BSANPs dispersed in 20 mL of distilled water. The mixture was kept under continuous shaking for 24 h, after which the drug-loaded nanoparticles were separated [11]. The drug loading capacity is calculated using Eq. (1);

$$\text{Loading capacity } (\%) = \frac{W(\text{drug}-\text{loaded})}{W(TiO_2\text{NPS})} \times 100\% \quad (1)$$

where W (drug-loaded) is the weight of vinorelbine loaded, and W TiO_2@BSANPs is the weight of TiO_2NPs. Each experiment was performed in triplicate, and the results are presented as mean values with their corresponding standard deviations. The concentration of VRL in the supernatant was quantified using a standard calibration curve prepared from a series of known drug concentrations (absorbance range: 0–3.5 µg/mL).

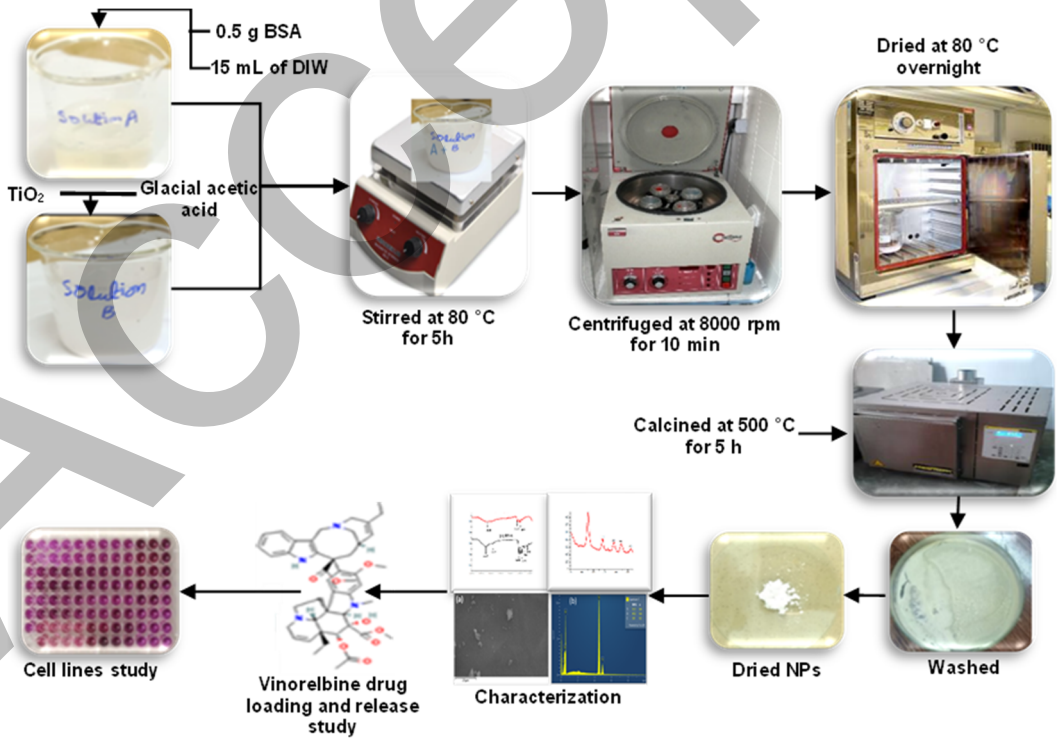

Fig 1. Overall layout of the research work

Drug release

Drug release was determined by suspending VRL-loaded TiO_2@BSANPs in 50 mL of 0.1 M phosphate buffer (pH 7.4 and 5.5) at 37 °C under continuous shaking for 60 h. At 1-h intervals, 3 mL samples were withdrawn and replaced with fresh buffer to maintain constant volume and sink conditions [12]. The drug release percentage is estimated using Eq. (2);

$$\text{VRL release (\%)} = \frac{\text{W(drug release)}}{\text{W(total drug)}} \times 100\% \quad (2)$$

where W (drug released) is the amount of VRL released, and W (total drug) is the weight of VRL loaded on TiO_2@BSANPs.

Cytotoxicity assay

The MTT assay was used to evaluate cell proliferation of TiO_2@BSANPs, VRL, and TiO_2@BSA@VRLNPs. The MCF-7 (6×10^3 cells/well) 6-well µL plates were seeded with cells according to the manufacturer's guidelines, then maintained in a 5% (v/v) CO_2 atmosphere in a 95% (v/v) humidified environment at 37 °C overnight. The cells were then subjected to varying concentrations of drug-loaded NPs (200 to 6.25 µg/mL). MTT reagent (20 µL) was added to each well after 24 h; the wells were then incubated for an additional 4 h. The purple formazan crystals were dissolved by adding 100 µL of DMSO to each well [13]. A microplate reader was used to measure absorbance at 570 nm.

■ RESULTS AND DISCUSSION

UV–Vis Spectroscopy of TiO_2@BSANPs

UV-vis spectroscopy is one of the most crucial characterization methods for understanding the formation of nanoparticles. The absorption spectra showed an intense band with λ_{max} at 361 nm, which indicates the successful synthesis of TiO_2@BSANPs (Fig. 2). Similar observation for TiO_2NPs with an absorption edge between 350 and 400 nm has been reported, that corresponds to the intrinsic charge transfer transition from the oxygen 2*p* valence band to the titanium 3*d* conduction band, a characteristic feature of its electronic structure [14].

FTIR Spectroscopy

FTIR spectroscopy was employed to investigate the functionalization of TiO_2NPs with BSA (Fig. 3(ai)). In the BSA spectrum, characteristic bands were observed at 3435 (N–H stretching of primary amines), 2958 (C–H stretching), 1654 (amide I, α-helix structure), 1454 (–CH_2– stretching), 1384 (C–N stretching), 124 (C=S), and 701 cm^{-1} (NH_2/NH wagging). The TiO_2@BSANPs spectrum (Fig. 3(aii)) exhibits bands at 3354 and 1621 cm^{-1}, indicating the presence of O–H groups and surface-adsorbed water, respectively [15], the peak at 621 cm^{-1} confirms the presence of anatase TiO_2. A slight shift in the 1454 cm^{-1} peak to 1452 cm^{-1} further confirms the successful surface functionalization of TiO_2NPs with BSA.

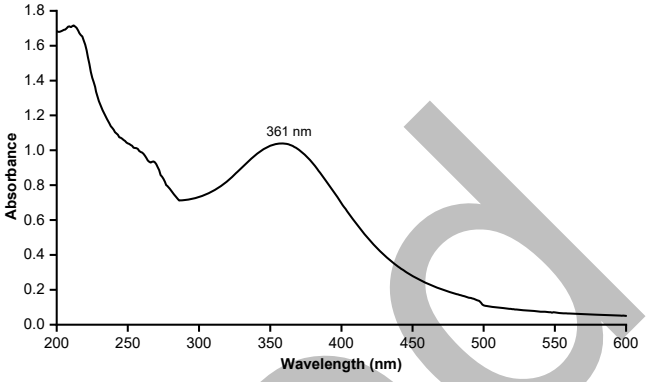

Fig 2. UV-vis spectrum of TiO_2@BSANPs

Fig. 3(bi) and (bii) demonstrate the FTIR of VRL and TiO_2@BSA@VRLNPs. In Fig. 3(bii), the spectrum of TiO_2@BSA@VRLNPs, some peaks were slightly shifted, while others had disappeared, indicating the possible interactions between VRL and TiO_2@BSANPs. In Fig. 3(bi) spectra the high intensity wide bands of VRL at around 3357 (O–H, NH stretching), 2958 (C–H stretching of methyl), 1720 (C=O stretching), 1431 (–CH_2– stretching), 1260 (C–H stretching of COOR), 832 (out of plane C–H bending vibration), and 1038 cm^{-1} (C–OH stretching deformation). These peaks were also observed in the spectrum of TiO_2@BSA@VRLNPs peaks at 3337, 1455, 1215, and 813 cm^{-1}, which are slightly shifted; the band at 621 cm^{-1} is of TiO_2@BSANPs. The band at 1720 cm^{-1} in the spectrum of VRL was shifted to 1646 cm^{-1}, while the peaks at 2958 and 1038 cm^{-1} in the spectrum of VRL drug completely disappeared in the spectra of TiO_2@BSA@VRLNPs, confirming that the drug was successfully loaded into the TiO_2@BSANPs.

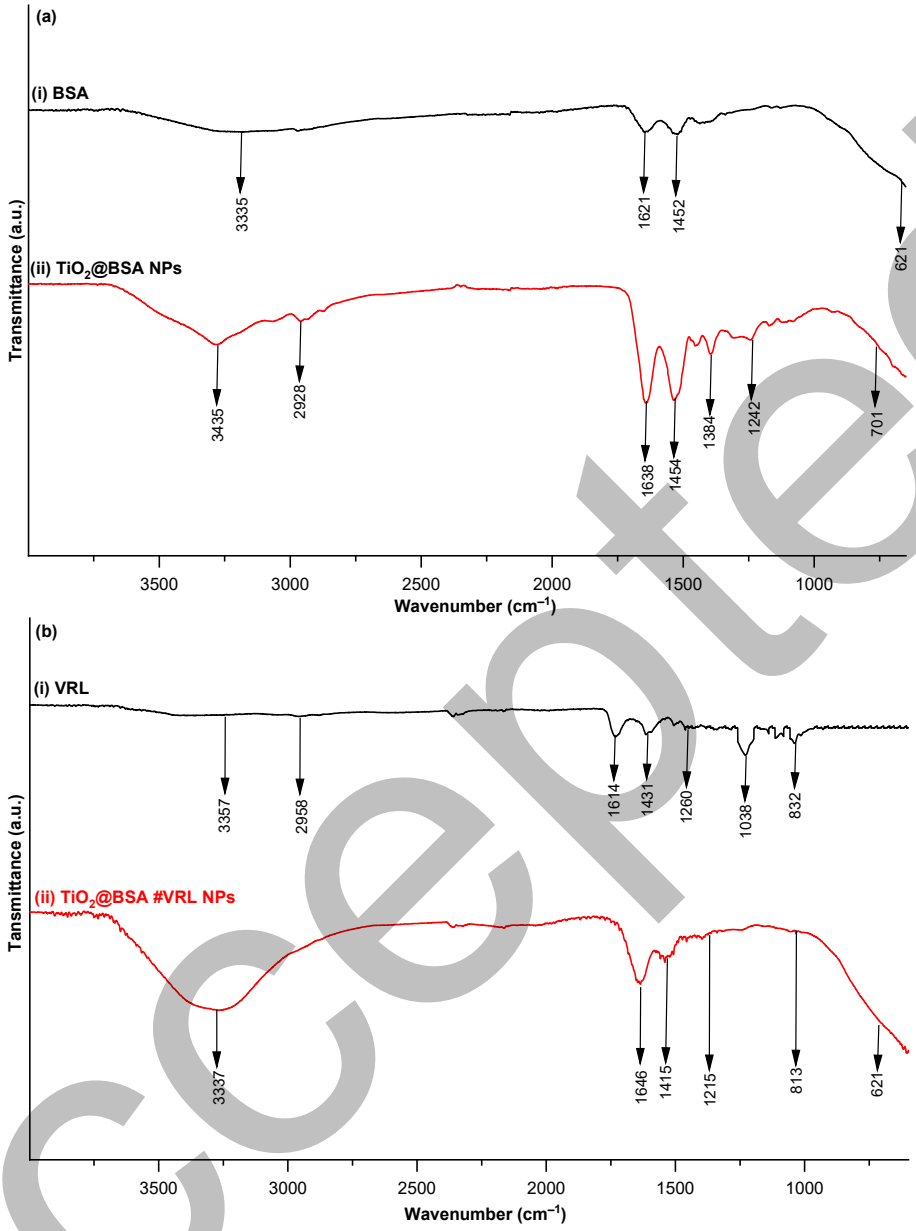

Fig 3. FTIR spectra of (a) (i) BSA and (ii) TiO_2@BSANPs, and (b) (i) VRL and b(ii) TiO_2@BSA@VRLNPs

Morphological and Elemental Analysis

The microstructure of TiO_2@BSANPs was examined using FE-SEM (Fig. 4(a)), revealing uniformly dispersed, spherical nanoparticles with smooth surfaces, characteristic of the anatase phase. Elemental composition was determined by energy-dispersive X-ray spectroscopy (EDX) (Fig. 4(b)), confirming the presence of titanium (Ti) and oxygen (O) with weight percentages of 51.1 and 45.2%, respectively, indicating the successful synthesis of TiO_2-based nanocomposites.

XRD

XRD analysis was performed to assess the crystallinity and average crystallite size of TiO_2@BSANPs. Diffraction peaks at 2θ values of 25.42°, 37.91°, 48.14°, 54.48°, 60.51°, and 68.81° correspond to the 101, 112, 200, 105, 204, and 116 planes, respectively, as illustrated in Fig. 5. Crystallite size (L) was calculated using the Scherrer equation in Eq. (3).

$$L = \frac{k\lambda}{\beta \cos\theta} \quad (3)$$

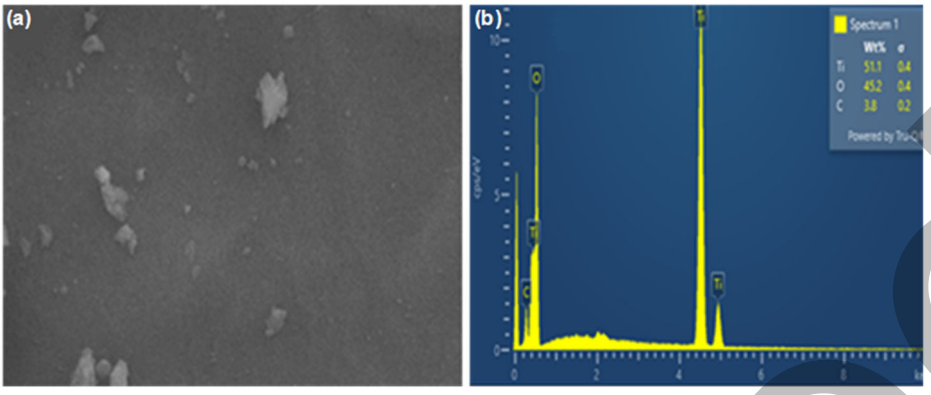

Fig 4. (a) FE-SEM images of TiO_2@BSANPs and (b) EDX analysis of TiO_2@BSANPs

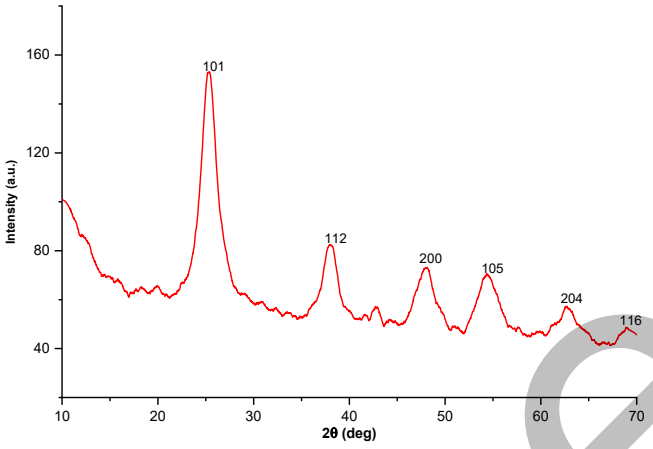

Fig 5. XRD of TiO_2@BSANPs

The Scherrer constant (k) was taken as 0.94, with the X-ray wavelength (λ) of 1.5418 Å (Cu Kα). Here, θ is the Bragg angle, and β is the full width at half maximum (FWHM). The average crystallite size was estimated to be ~20 nm. The most intense peak at 2θ = 25.23° corresponds to the anatase phase, with the predominant 101 plane.

Dynamic Light Scattering Study of TiO_2@BSANPs

Dynamic light scattering (DLS) is commonly employed to determine the size of nanoparticles in suspension. The particle sizes obtained by DLS are generally larger than those measured by techniques such as XRD. DLS accounts for the hydrodynamic diameter, which includes the solvation layer surrounding the particles in the aqueous medium. Consequently, DLS typically yields comparatively larger size values for NPs [16]. DLS analysis of TiO_2@BSANPs in solution (Fig. 6(a)) shows an average size of approximately 396 nm. Additionally, the zeta potential represents the electrostatic charge at the interface between the solid surface of nanoparticles and their surrounding liquid medium. Fig. 6(b) presents the zeta potential values of TiO_2@BSANPs. Measurements were conducted at room temperature. The NPs exhibited a zeta potential of −29 mV, indicating strong electrostatic repulsion among the particles, which contributes to their stability in suspension. Particles exhibiting zeta potential values greater than +30 mV or less than −30 mV are generally regarded as stable, as previously reported in the literature [17].

Drug Loading and Release

In the drug loading study, the concentration was taken in the range of 1 and 6 µg/mL. As the concentration increased, the loading capacity also increased, reaching an optimum of 5 µg/mL, which was selected as the optimal concentration for this study. Further increases in VRL concentration led to saturation of drug loading, confirming that 5 µg/mL was the optimum concentration, as shown in Fig. 7(a). The drug release profile of TiO_2@BSA@VRLNPs was evaluated at pH 5.5 (tumor-like acidic environment) and pH 7.4 (normal physiological condition), as shown in Fig. 7(bi, bii). At pH 7.4, the cumulative drug release after 48 h was only 20%. In contrast, at pH 5.5, a significantly higher release (98%, $p < 0.05$) was observed, characterized by an initial burst followed by a sustained release phase. These results indicate enhanced drug release under acidic conditions, which is attributed to the protonation of polar functional groups in both the

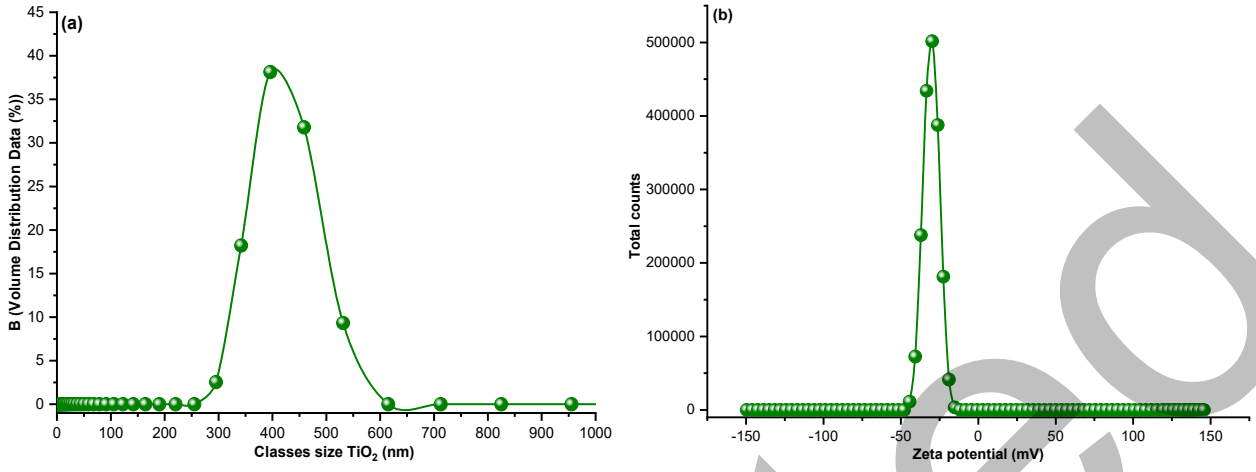

Fig 6. (a) DLS and (b) zeta potential of TiO_2@BSANPs

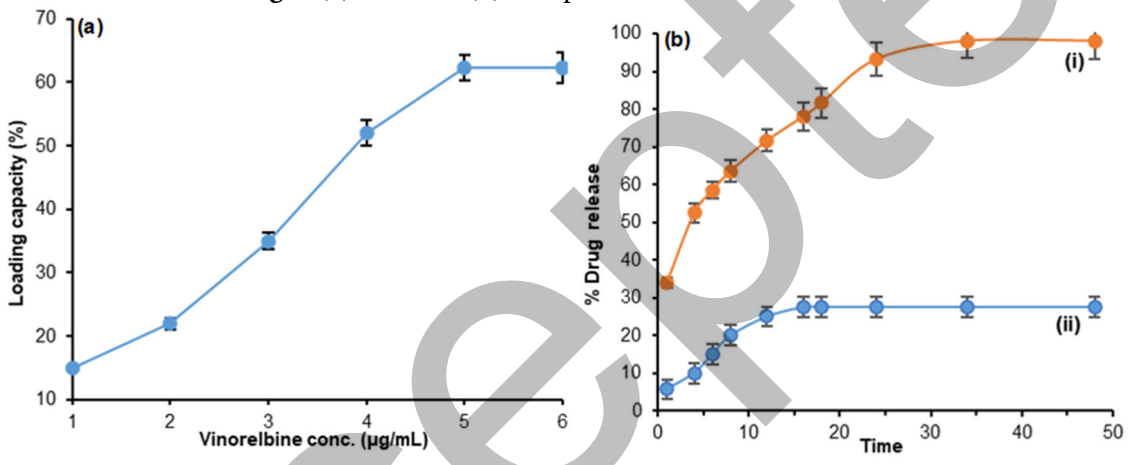

Fig 7. (a) Drug Loading capacity of VRL and (b) drug release profiles of TiO_2@BSA@VRLNPs at pH (i) 5.5 and (ii) 7.4

drug and nanoparticle components. This leads to repulsive forces and disruption of drug-nanoparticle interactions, accelerating release. The pH-sensitive behavior ensures that drug release is explicitly triggered in the tumor microenvironment, thereby minimizing off-target effects and maintaining a high drug concentration at the tumor site. The sharper release slope in the early stages is due to a higher concentration gradient, which gradually diminishes over time.

Kinetics Modeling Study

Standard mathematical models were employed to gain a deeper understanding of the drug release mechanism from TiO_2@BSANPs. Understanding the factors that influence the release profile is crucial for designing effective drug delivery systems. Drug release from nanocarriers can occur through various mechanisms, including erosion, swelling, diffusion, and degradation of the carrier material [18]. In this study, the release of VRL at both physiological and tumor-relevant pH levels was analyzed using four kinetic models: zero-order, first-order, Higuchi, and Korsmeyer-Peppas. The model fit was assessed by the regression coefficient (R^2), where a higher value indicates a stronger correlation with the release mechanism (Table 1). Graphs were plotted for each model as shown in Fig. 8. The prediction of drug release from nanoparticles involved fitting the data to various kinetic models. The zero-order model, which assumes a constant release rate independent of drug concentration, showed a good fit at pH 7.4 with a R^2 of 0.9675. This suggests that VRL release from TiO_2@BSANPs is steady over time, potentially due to the nanoparticles acting as nano-reservoirs, maintaining a constant concentration gradient. Additionally, the Higuchi model, which describes drug

Table 1. Regression coefficient (R^2) values represent kinetic models for VRL release from VRL-based matrices

	Kinetic models					
	Zero-order	First-order	Higuchi		Korsmeyer	Peppas
	R^2	R^2	R^2	R_H	R^2	N
pH 7.4	0.9675	0.9230	0.9714	10.80	0.9159	0.44
pH 5.5	0.9501	0.9363	0.9901	31.56	0.9379	0.82

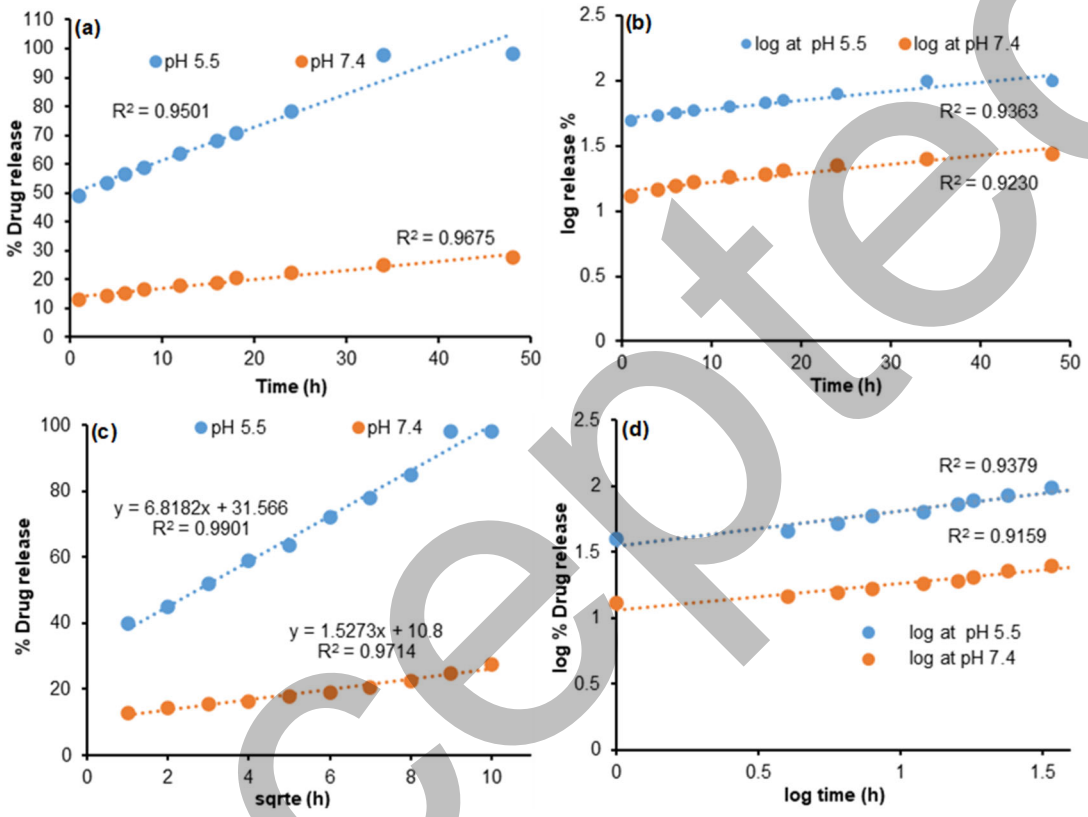

Fig 8. Kinetic fitting using (a) zero-order, (b) first-order, (c) Higuchi, and (d) Korsmeyer-Peppas drug diffusion models

release as a diffusion process proportional to the square root of time, showed an excellent correlation (R^2 = 0.9901 at pH 5.5 and R^2 = 0.9714 at pH 7.4). This confirms diffusion as the primary mechanism of release. An initial burst, likely due to surface-bound drug, was followed by sustained release as VRL diffused from the nanoparticle matrix.

The Korsmeyer-Peppas model further supported this, with the release exponent (n) indicating quasi-Fickian or anomalous transport mechanisms. Similar findings were reported by using BSA-based nanoparticles [19] and using liposome silver nanocomposites [20]. Our results confirm that VRL release from TiO_2@BSANPs is diffusion-driven and aligns closely with the Higuchi model, with contributions from non-Fickian transport as indicated by the Korsmeyer-Peppas model.

MTT Cytotoxicity assay for TiO_2@BSANPs, VRL, TiO_2@BSA@VRLNPs

The MTT assay results presented in Fig. 9 illustrate the dose-dependent cytotoxicity of TiO_2@BSANPs, free VRL, and TiO_2@BSA@VRLNPs against MCF-7 breast cancer cells at concentrations ranging from 6.25 to 200 µg/mL. TiO_2@BSA@VRLNPs demonstrated enhanced cytotoxicity compared to free VRL, likely due to improved cellular uptake and sustained release. Although

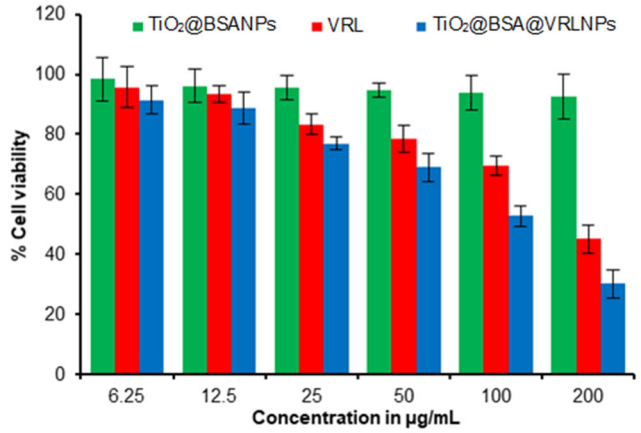

Fig 9. *In vitro* cytotoxicity of TiO_2@BSANPs, VRL, TiO_2@BSA@VRLNPs against breast cancer cell line MCF-7 according to the MTT test

TiO_2@BSANPs alone showed minimal cytotoxicity, it was not statistically significant. Similarly, it has been reported that aptamer-functionalized VRL-loaded nanoparticles (AP NP/VRL) significantly reduce cell viability in MDA-MB-231 cells more effectively than both NP/VRL and free VRL, highlighting the benefit of targeted delivery through nucleolin-mediated endocytosis. However, in non-cancerous MCF-10A cells, no significant cytotoxic advantage was observed for AP NP/VRL, indicating selective action toward cancer cells. In another study by folic acid-functionalized TiO_2-PEG nanocarriers (FA-PEG-TiO) loaded with paclitaxel (PAC) exhibited controlled drug release and notable dose-dependent cytotoxicity in HepG2 liver cancer cells. The IC_{50} values confirmed increasing efficacy in the order: pure TiO_2 (61.25 µg/mL) > TiO_2-PEG-FA (59.6 µg/mL) > TiO_2-PEG-FA-PAC (22.75 µg/mL). The enhanced cytotoxicity of the PAC-loaded FA-functionalized NPs was attributed to receptor-mediated uptake via folate receptors, which enabled improved drug delivery and a therapeutic response.

■ CONCLUSION

Herein, TiO_2NPs were successfully synthesized and functionalized with biocompatible BSA, thereby enhancing their functional and physicochemical properties under physiological conditions. The synthesized TiO_2@BSANPs were subsequently loaded with VRL, and their pH-responsive drug release behavior was investigated. The results revealed a significantly higher drug release (98%) at acidic pH (5.5) compared to physiological pH, indicating their potential for tumor-targeted delivery. Furthermore, MTT assay results demonstrated that VRL-loaded TiO_2@BSANPs exhibited enhanced cellular uptake and cytotoxicity compared to free VRL. Kinetic modeling confirmed that the drug release data were well-fitted to the Korsmeyer-Peppas and Higuchi models, suggesting a diffusion-controlled release mechanism.

■ ACKNOWLEDGMENTS

The authors acknowledge the facilities provided by the Center of Excellence, University of Sindh, as well as the technical support provided by the Process Simulation and Modeling Research Group, Department of Chemical Engineering, Mehran University of Engineering and Technology, Jamshoro.

■ CONFLICT OF INTEREST

All authors have no conflict of interest.

■ AUTHOR CONTRIBUTIONS

Sanam Rahujo conceptualized, synthesized, designed experiments, and conducted data collection and analysis. Hassan Imran Afridi and Zafar Ali accomplished the characterization. Abdul Qadeer Laghari and Masroor Abro performed data analysis and formatting editing throughout the draft. Noshad Razzaque, Imamdin Chandio, and Noorzaman interpreted the results. Farah Naz and Olcay Mert supervised the whole project and reviewed the draft. All authors read, revised, and approved the final version of the manuscript.

■ REFERENCES

[1] Mehrotra, R., and Yadav, K., 2022, Breast cancer in India: Present scenario and the challenges ahead, *World J. Clin. Oncol.*, 13 (3), 209–218.

[2] Dongsar, T.T., Dongsar, T.S., Abourehab, M.A.S., Gupta, N., and Kesharwani, P., 2023, Emerging application of magnetic nanoparticles for breast cancer therapy, *Eur. Polym. J.*, 187, 111898.

[3] He, F., Yu, W., Fan, X., and Jin, B., 2017, *In vitro* cytotoxicity of biosynthesized titanium dioxide nanoparticles in human prostate cancer cell lines, *Trop. J. Pharm. Res.*, 16 (12), 2793-2799.

[4] Bai, S., Yang, N., Wang, X., Gong, F., Dong, Z., Gong, Y., Liu, Z., and Cheng, L., 2020, Ultrasmall iron-doped titanium oxide nanodots for enhanced sonodynamic and chemodynamic cancer therapy, *ACS Nano*, 14 (11), 15119–15130.

[5] Salehiabar, M., Nosrati, H., Davaran, S., Danafar, H., and Manjili, H.K., 2018, Facile synthesis and characterization of l-aspartic acid coated iron oxide magnetic nanoparticles (IONPs) for biomedical applications, *Drug Res.*, 68 (5), 280–285.

[6] Younis, A.B., Haddad, Y., Kosaristanova, L., and Smerkova, K., 2023, Titanium dioxide nanoparticles: Recent progress in antimicrobial applications, *WIREs Nanomed. Nanobiotechnol.*, 15 (3), e1860.

[7] Hossain, N., Mobarak, M.H., Islam, M.A., Hossain, A., Al Mahmud, M.Z., Rayhan, M.T., and Chowdhury, M.A., 2023, Recent development of dental implant materials, synthesis process, and failure–A review, *Results Chem.*, 6, 101136.

[8] Agarwala, P., Bera, T., and Sasmal, D.K., 2022, Molecular mechanism of interaction of curcumin with BSA, surfactants and live *E. Coli* cell membrane revealed by fluorescence spectroscopy and confocal microscopy, *ChemPhysChem*, 23 (18), e202200265.

[9] Al-Khazraji, A.M.A., 2024, Synthesis, characterization, and evaluation of MCF-7 (breast cancer) for Schiff, Mannich bases, and their complexes, *Indones. J. Chem.*, 24 (1), 213–227.

[10] Marycleopha, M., Yaou Balarabe, B., Adjama, I., Moussa, H., Anandaram, H., and Abdoul Razak, M.W., 2024, Anhydrous sol-gel synthesis of TiO_2 nanoparticles: Evaluating their impact on protein interactions in biological systems, *J. Trace Elem. Miner.*, 7, 100114.

[11] Peng, H.H., Hong, D.X., Guan, Y.X., and Yao, S.J., 2019, Preparation of pH-responsive DOX-loaded chitosan nanoparticles using supercritical assisted atomization with an enhanced mixer, *Int. J. Pharm.*, 558, 82–90.

[12] Kim, Y., Park, E.J., Kim, T.W., and Na, D.H., 2021, Recent progress in drug release testing methods of biopolymeric particulate system, *Pharmaceutics*, 13 (8), 1313.

[13] Chelliah, R., Elahi, F., and Oh, D.H., 2022, "Screening for Antiviral Activity: MTT Assay" in *Methods in Actinobacteriology*, Springer, New York, NY, US, 419–421.

[14] Nematov, D., 2024, Titanium dioxide and photocatalysis: A detailed overview of the synthesis, applications, challenges, advances and prospects for sustainable development, *J. Mod. Green Energy*, 3, 6.

[15] Dhavale, R.P., Dhavale, R.P., Sahoo, S.C., Kollu, P., Jadhav, S.U., Patil, P.S., Dongale, T.D., Chougale, A.D., and Patil, P.B., 2021, Chitosan coated magnetic nanoparticles as carriers of anticancer drug Telmisartan: pH-responsive controlled drug release and cytotoxicity studies, *J. Phys. Chem. Solids*, 148, 109749.

[16] Bagheri, S., Shameli, K., and Abd Hamid, S.B., 2013, Synthesis and characterization of anatase titanium dioxide nanoparticles using egg white solution via sol-gel method, *J. Chem.*, 2013(1), 848205.

[17] Bhagat, S., Shaikh, H., Nafady, A., Sirajuddin, S., Sherazi, S.T.H., Bhanger, M.I., Shah, M.R., Abro, M.I., Memon, R., and Bhagat, R., 2022, Trace level colorimetric Hg^{2+} sensor driven by *Citrus japonica* leaf extract derived silver nanoparticles: green synthesis and application, *J. Cluster Sci.*, 33 (5), 1865–1875.

[18] Carone, A., Emilsson, S., Mariani, P., Désert, A. and Parola, S., 2023, Gold nanoparticle shape dependence of colloidal stability domains, *Nanoscale Adv.*, 5 (7), 2017–2026.

[19] Milani Fard, M., and Milani Fard, A.M., 2022, Modeling drug release, *Eurasian J. Sci. Technol.*, 2 (1), 14–33.

[20] Jayachandran, P., Ilango, S., Suseela, V., Nirmaladevi, R., Shaik, M.R., Khan, M., Khan, M., and Shaik, B., 2023, Green synthesized silver nanoparticle-loaded liposome-based nanoarchitectonics for cancer management: *In vitro* drug release analysis, *Biomedicines*, 11 (1), 217.